CONFERENCE PRE-PRINT

DRIFT FLOWS IMPACT ISLAND DIVERTOR OPERATION IN WENDELSTEIN 7-X

C. KILLER, D. CIPCIAR, Y. GAO, O. GRULKE, A. PANDEY, V. PERSEO, F. REIMOLD, F. SCHARMER, A. VON STECHOW, M. VECSEI
Max Planck Institute for Plasma Physics
Greifswald, Germany
Email: carsten.killer@ipp.mpg.de

S.G. BAEK, S. BALLINGER, J. TERRY MIT-PSFC Cambridge, MA, USA

D.M. KRIETE Auburn University Auburn, AL, USA

Abstract

The island divertor in Wendelstein 7-X employs a chain of stationary magnetic islands to separate the confined plasma from the divertor targets. In this configuration, the scrape-off layer (SOL) exhibits complex, counter-streaming parallel and perpendicular plasma flows. The perpendicular flows are likely ExB drift flows, oriented predominantly in the poloidal direction, and feature velocities of several km/s. Due to the long parallel connection length in the island divertor, such flows can well compete with parallel transport on the open field lines to the divertor targets, significantly altering heat and particle flux patterns. Reversed field experiments clearly indicate the key role of effect of drift flows for fluxes to the divertors and parallel flow patterns. Further, and likely related, non-monotonic profiles of electron temperature and density are observed in the scrape-off layer. These effects cannot be reproduced by state-of-the-art models such as the leading 3D mean-field transport code EMC3-EIRENE, as the drift flow physics are not yet included. The mismatch between experiment and simulation poses a critical challenge for optimizing W7-X divertor operation at higher heating powers and for the design of future stellarator reactors. These findings underscore the need for incorporating drift physics into 3D transport models to enable predictive design of stellarator divertors.

1. INTRODUCTION

Stellarators are recently emerging as increasingly attractive alternatives to tokamak fusion plants, with the optimized stellarator Wendelstein 7-X (W7-X) currently exploring the path towards reactor-relevant scenarios. The most mature exhaust concept for stellarators is the island divertor, which was tested in W7-AS [1,2] and is now in operation in W7-X [3]. There, the vacuum magnetic field is designed such that a stationary chain of resonant magnetic islands exists at the plasma edge, separating the confined plasma from the divertor targets. In W7-X, there are 4, 5, or 6 islands depending on the chosen magnetic configuration and the associated resonance of the rotational transform. The magnetic field pitch angle is very shallow in the island divertor scrape-off layer (SOL) which leads to long parallel connection lengths of several 100m to the targets. The divertor targets are toroidally discontinuous, resulting in the existence of shadowed regions of very short connection lengths between the targets, which are purely filled with particles and energy by perpendicular transport [4].

These unique properties of the island divertor SOL result in additional physics phenomena beyond tokamaks SOL physics, e.g. non-monotonic radial electron temperature profiles [5, 6], drift flows associated to magnetic islands [7, 8, 9], and complex parallel flow structures [10, 11]. As a consequence, heat and particle exhaust to the divertor is affected, resulting in unintended heat loads to vulnerable components [12, 13] and generally significant asymmetries between upper and lower divertors [11, 14]. To date, these observation cannot be fundamentally reproduced with numerical models: most edge transport models for fusion plasmas are two-dimensional and rely on the axisymmetry of tokamaks. The only established 3D edge transport code to date is EMC3-EIRENE, which

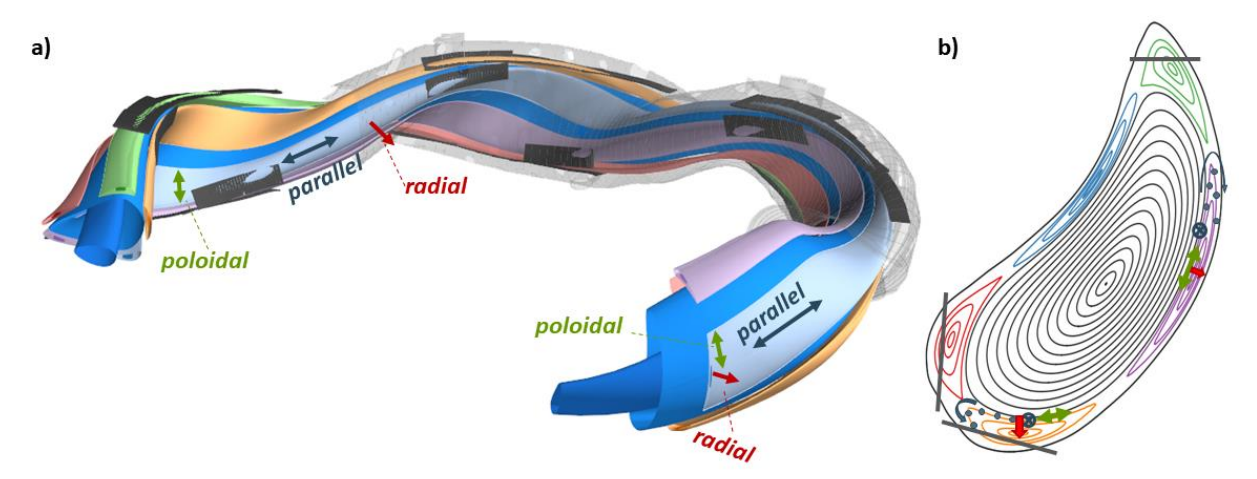


FIG 1 a) 3D sketch of W7-X "standard configuration" with core and edge flux surfaces of the main plasma (blue), five magnetic islands (colored ribbons surrounding the main plasma), modular divertor targets (black, shown for 3 out of 5 modules), plasma vessel outline (transparent gray, shown for 2 out of 5 modules). b) Poincare cross section showing flux surfaces of the main plasma (black) and the five magnetic islands (colored), and divertor targets (black). For two islands, the principal geometric directions are sketched: parallel on the field lines of island flux surfaces (dark green), poloidal / bi-normal direction on the island flux surfaces (light green), radially perpendicular to island flux surfaces (red)

can simulate the full 3D geometry of W7-X [15]. However, it does not self-consistently treat perpendicular turbulent transport, and, notably, does not include drifts such as ExB or diamagnetic drifts. However, drift transport is expected to be particularly relevant at low pitch angles such as found in W7-X. As a consequence, no detailed global match of simulation results with experiments is readily achieved [16, 17], although specific questions can well be addressed [10, 15, 18, 19, 20].

The lack of a 3D edge transport code with drifts is an issue for the divertor development of future stellarators on the path to reactors. In this presentation, an overview of experimentally observed drift effects and their implications for divertor operation in W7-X is given.

2. THE ISLAND DIVERTOR SOL GEOMETRY AND ITS EFFECT ON DRIFT TRANSPORT

The effects of perpendicular transport in the SOL of W7-X are closely related to the 3D island divertor geometry. A 3D sketch of W7-X is shown in Fig. 1a), where the islands are shown as colored ribbons that surround the main plasma (blue). The divertor modules (black) intersect the magnetic islands at discrete toroidal positions. The principal directions for plasma transport are indicated both in the 3D plot in Fig. 1a) and the Poincare cross section in Fig. 1b): parallel to the magnetic field (dark green), poloidal/bi-normal on the island flux surfaces (light green), and radially perpendicular to island flux surfaces (orange).

For the parallel direction, the individual markers on the flux surface in Fig. 1b) indicate the intersection points after one full toroidal turn of the field line. Due to the rotational transform $\iota/2\pi = 1$, the field line stays in the same island and ends up slightly displaced on its flux surface. This small poloidal displacement is approximately given by $2\pi R\Theta$ where R is the major radius and Θ is the island magnetic pitch angle, which is on the order of 10^{-3} in W7-X, i.e. much smaller than in tokamaks where $\Theta \sim 10^{-1}$ [20, 21].

The geometric directions in Fig. 1 are associated with very different scale lengths regarding the proximity to divertor targets. This is highlighted in Fig. 2, which shows a close-up view of a lower divertor module and in addition presents the magnetic connection length to the targets color-coded. Starting from a position close to the last closed flux surface (LCFS), it takes a field line several 100m (i.e. multiple toroidal turns, indicated by the individual small arrows) to reach the divertor plate. Traveling perpendicular to the magnetic field on that same flux surface, the distance is just some 10cm (green in Fig. 2). This transport direction is invoked by ExB drifts of electric fields that are perpendicular to the magnetic island flux surfaces (assuming constant potential on each flux surface for simplicity in the sketch in Fig. 2).

Non-monotonic radial electric fields across the islands and associated poloidal ExB flows have repeatedly been reported in W7-X with typical (measured or expected) flow velocities of some km/s [7, 9, 22, 23]. Effects agreeing with this picture are seen as up-down asymmetries in divertor heat fluxes [14] and radiation distribution [24], and

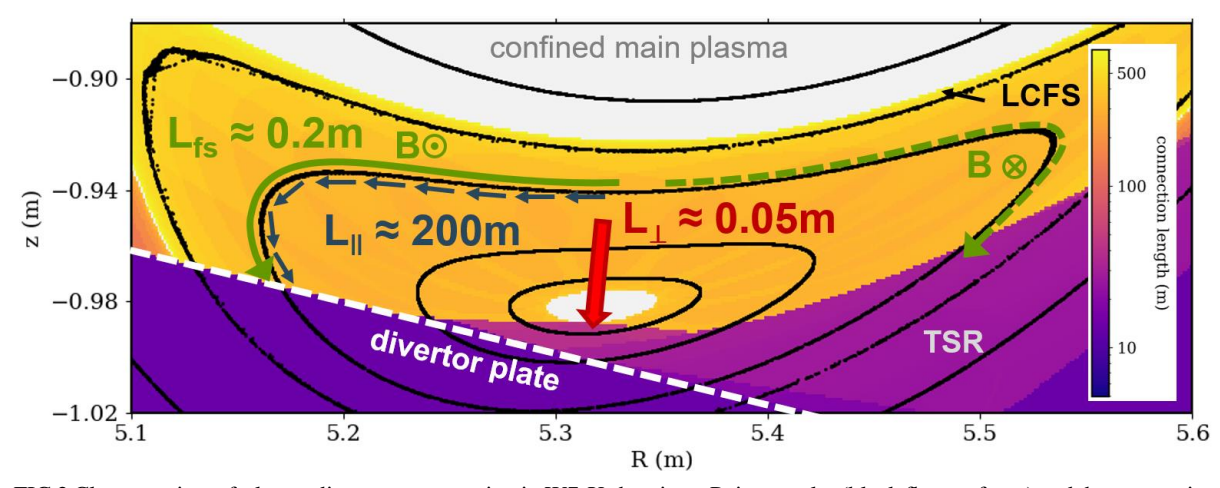


FIG 2 Close-up view of a lower divertor cross section in W7-X showing a Poincare plot (black flux surfaces) and the connection length to the targets (color coded). In addition, three principal directions for heat and particle transport are indicated along with their typical scale length from a position close to the LCFS to the divertor.

modification of the parallel flow structures [11]. Based on the direction of the magnetic field (and for simplicity assuming constant electric potential on island flux surfaces), the drift flow points either directly towards the target (as sketched in Fig. 2), or into the "target shadow" region" (TSR), corresponding to the purple part on the right hand side of Fig. 2. This region has short connection lengths of ~10m as it is in the shadow between two discrete divertor modules. Hence, it has no parallel connection to the separatrix, and as a consequence the TSR is filled only via perpendicular transport. In earlier field reversal experiments, a particularly strong change of divertor loads associated to the TSR have been observed, indicating a major role of drift effects in filling the TSR [11, 14].

Finally, in the direction normal to the confined flux surfaces, the distance to the target is just some cm (red in Fig. 2). This transport channel would be most effective in terms of the short physical distance to the target, but has typically much lower particle fluxes: Turbulent transport is found to lead to rather low diffusion coefficients of D=0.2m/s² [25] which was recently picked up by simulations works [16] but is smaller than the previously assumed values of D=0.5m²/s [15] to D=1m²/s [18]. Further, SOL turbulence in W7-X does not exhibit intermittent radial transport of blob-filaments that is known from tokamaks [25, 26, 27]. Radial ExB drifts from poloidal electric fields [11] are conceivable but have not been experimentally identified yet [23].

3. DIRECT OBSERVATION OF DRIFT FLOWS

The most direct observation of drift flows in W7-X is done with Gas Puff Imaging (GPI) and reciprocating electric probes.

3.1. Gas Puff Imaging (GPI)

GPI is based on fast imaging of H- α emission from a localized gas-puff [28]. Using spatio-temporal analysis, the propagation of fluctuating structures is obtained [9]. In the W7-X SOL, poloidal flows with typical velocities of several km/s are observed, while no discernible radial propagation is found [26]. Across the radial width of the SOL, the flows change sign, with between one and four flow reversal layers. A typical flow pattern in the "Standard" configuration of W7-X is presented in Fig. 3b) on top of the magnetic geometry (Poincare plot and connection lengths). Three major flow channels are found, R1) directed upwards in the main SOL (a few cm outside the LCFS), R2) directed downwards between the LCFS and the island O-point, R3) directed upwards in the O-point region of closed field lines. In the TSR, much smaller velocities are observed. The magnitude and spatial distribution of poloidal flow channels is highly sensitive to the magnetic field geometry, e.g. the size and position of magnetic islands [9, 23]

3.2. Reciprocating electric probes

A multi-pin Langmuir probe head on a reciprocating multi-purpose manipulator (MPM) [29] provides radial profiles of electron temperature T_e and density n_e as well as the floating potential V_f . Using a poloidal array of in total 29 probes, the time-averaged plasma properties in a 2D region of the SOL are obtained [23]. The probe

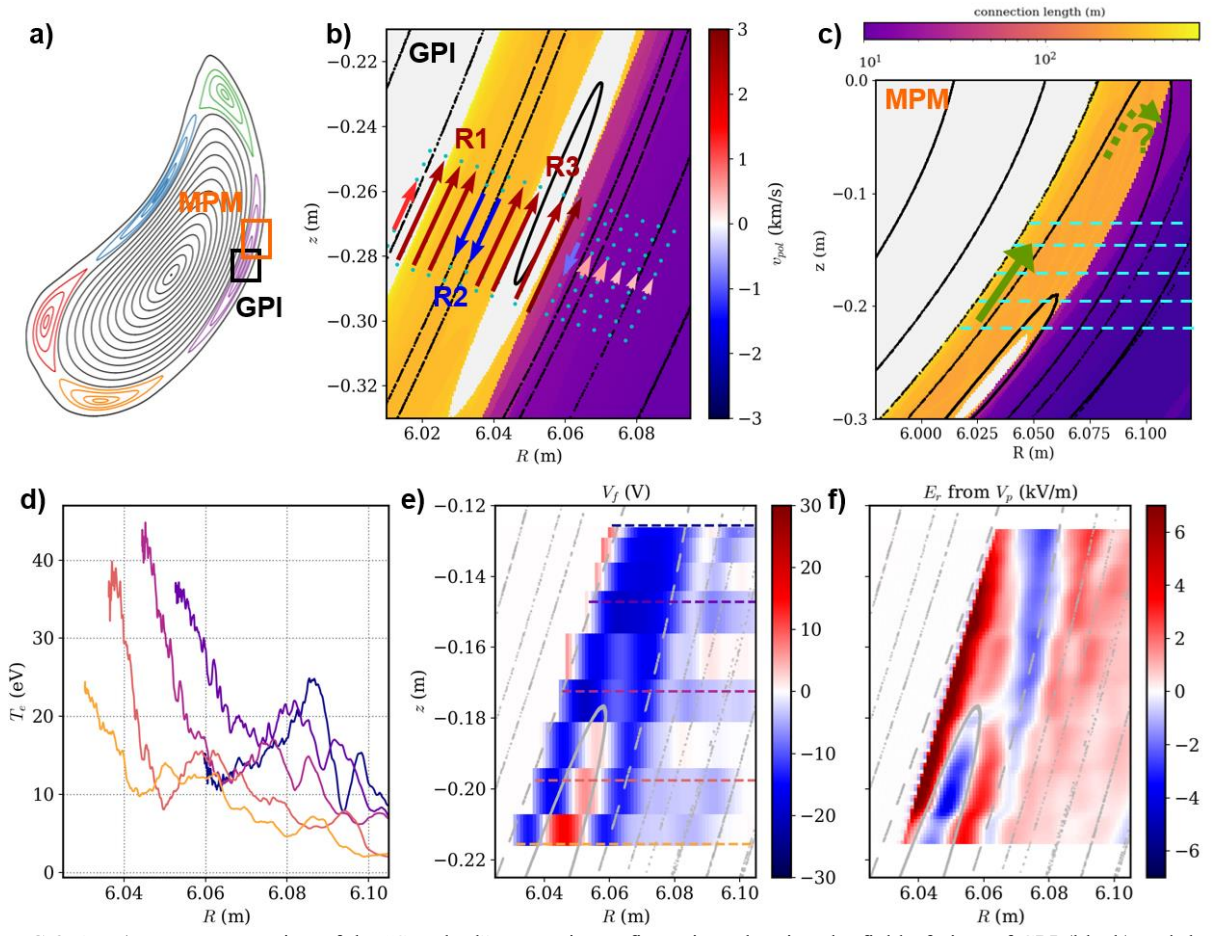


FIG 3 a) Poincare cross section of the "Standard" magnetic configuration, showing the field of view of GPI (black) and the region sampled by MPM reciprocating probes (orange). b) Typical poloidal velocity pattern measured by GPI (quiver plot). In the background, the magnetic structure including the connection length to the targets is plotted. The three black arrows indicate the measurement location for the results in Fig. 4 (different camera geometry). c) magnetic structure in MPM FoV. The cyan lines indicate region where electron temperature profiles (shown in d)) were sampled. The green arrow gives the ExB flow direction in forward field direction, see Fig. 2. d)-f) radial profiles of T_e, V_f, E_r from MPM Langmuir probe measurements. The five profiles in d) correspond to the dashed horizontal lines in c), e). Data is taken from W7-X program 20241210.45

system is installed in a stellarator-symmetric cross section to GPI, with a slight vertical displacement due to technical constraints, such that the fields of view are adjacent but do not overlap, see Fig. 3a) and 3c).

A typical result in "Standard" configuration of W7-X is shown in Fig. 3d-f): The electron temperature profiles in Fig. 3d) are taken by five triple Langmuir probes that are radially scanning the SOL at different poloidal positions, see dashed lines in Fig. 3c). Except for the uppermost probe, T_e decreases from higher values close to the LCFS and features a flat or even minimum region between the radial island center and the TSR. The floating potential in Fig. 3e), taken by 9 floating probes, follows the magnetic island geometry: Local maxima of V_f are observed around the central island flux surfaces and aligned with the TSR boundary, particularly pronounced for the upper probes around R = 6.08 m. Concomitantly, also the T_e profiles of the upper probes feature a local maximum at this position. From the T_e and V_f data, a 2D map of the plasma potential $V_p = V_f + 2.8 T_e$ is obtained, which then provides the radial electric field $E_r = -\nabla_r V_p$, see Fig. 3f). The radial electric field shows a layer of locally negative E_r and thus causes sheared poloidal plasma flows [23]. A detailed quantitative comparison of GPI and MPM drift flows has not been possible yet, as the flow patterns are highly sensitive on the plasma scenario and small details of the SOL magnetic geometry [9, 23].

4. DENSITY DEPENDENCE OF DRIFT FLOWS

In recent investigations on SOL drift flows in W7-X, the plasma density plays a key role, leading to smaller drift effects at higher densities. As reactor-relevant scenarios will focus on higher density scenarios, this section aims to broaden the understanding of the drift flow density dependence. [11] reports on particularly strong drift effects

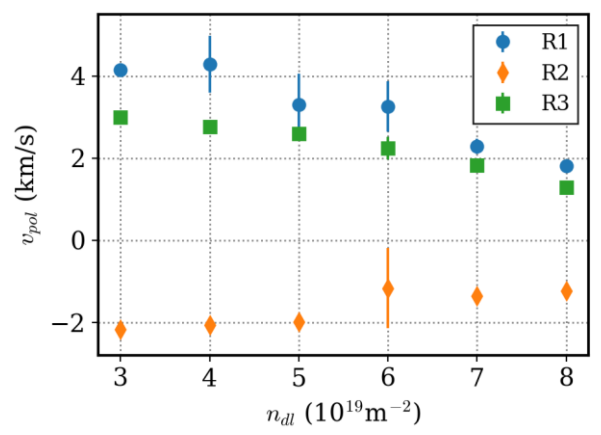


FIG 4 Poloidal flow velocities from gas puff imaging as a function of plasma density in magnetic standard configuration for three radial positions, see Fig. 3b).

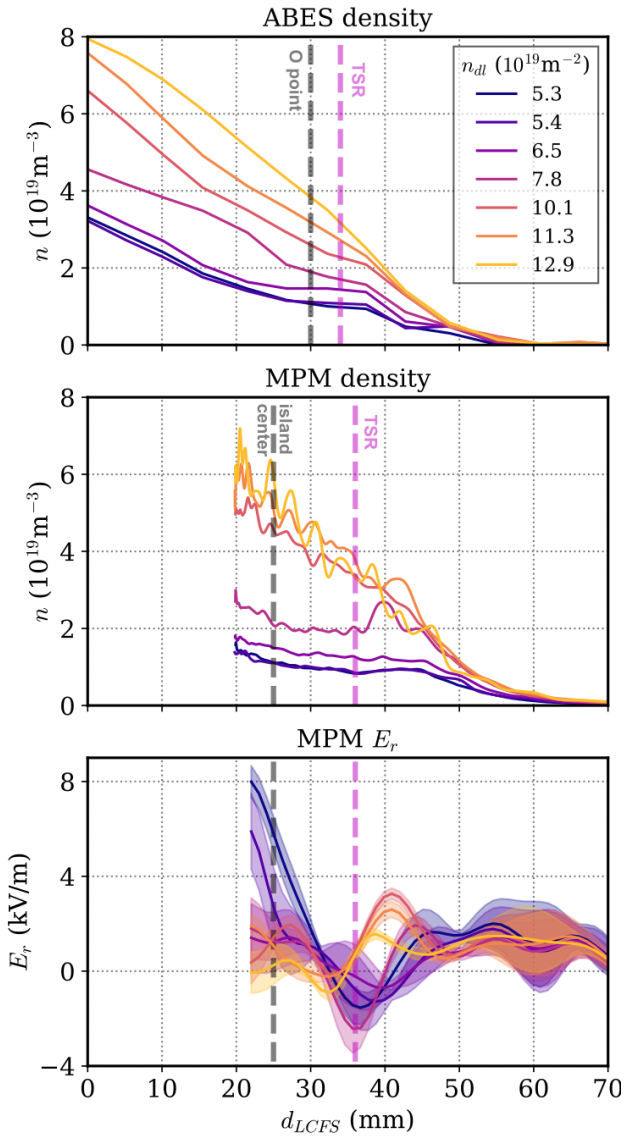


FIG 5 Radial profiles of plasma density and radial electric field in the SOL in magnetic standard configuration for a density scan at $P_{\rm ECRH} \approx 7 MW$. The gray dashed line represents the O point of the magnetic island (ABES) / the island center along the MPM axis, while the pink dashed line indicates the TSR boundary (transition from long to short connection lengths). Data is taken from experiments 20250408.59, 20250408.69.

at low plasma densities (n_{dl}~2e19m⁻²) where the SOL tends to be close to the sheath-limited regime with high divertor temperatures. For higher densities, the drift effects decrease, presumably along with the transition to a conduction-limited regime that features higher parallel Te gradients [11]. In [22], hollow SOL T_e profiles with a T_e minimum at the island O-point are also reported to be most pronounced at low densities. For n_{dl}>6e19 m⁻², the hollowness is lost, which is attributed to a decrease of E_r and thus ExB flow velocity [22]. In [30], an agreement of MPM probe measurements and EMC3-EIRENE is only found for n_{dl}>7e19 m⁻ ², and it is hypothesized that the mismatch at lower densities is due to the stronger drift effects (which are not included in EMC3-EIRENE).

4.3. **GPI measurements**

The density dependence of poloidal drift flows measured with GPI is presented in Fig. 4 for a large data base of gas puffs in the magnetic standard configuration in forward field direction for P_{ECRH}=4MW and small plasma currents (I_p<3kA), such that the magnetic island topology stays close to the vacuum case [31]. Three radial positions representative of the main flow patterns are selected for this analysis, see labels R1-R3 in Fig. 3b). For all three radial positions, the flow direction is constant as a function of plasma density, while the flow velocity magnitude continuously decreases towards higher densities. No threshold behaviour around specific density values is observed.

4.4. SOL density and E_r profile

SOL density profiles from the Alkali Beam Emission Spectroscopy (ABES) [32] and from reciprocating probes on the MPM [29] for a density scan are presented in Fig. 5. The experiments were again conducted in the magnetic standard configuration, at a heating power of $P_{\text{ECRH}} \approx 7MW$ to keep plasmas fully attached even at the highest densities. While the ABES measurement is taken in the outboard mid-plane of the bean shaped cross section of W7-X, right through the O-point of a magnetic island, the MPM probes the island 20cm above the O-point, see Fig. 3c). Still, both diagnostics show remarkably similar SOL density profiles during the core plasma density scan in Fig. 5, qualitatively and quantitatively. Particularly noteworthy is the flat density profile across the island for lower core densities, with a density shoulder just outside the TSR boundary (pink dashed line). The small radial discrepancy between density shoulder and TSR boundary might be due to the connection length (L_c) profile actually changing in two steps as seen in Fig. 3c), with a narrow region of $L_c\sim10$ m between the main SOL ($L_c\sim100$ m) and deeply shadowed ($L_c\sim1$ m) regions.

For higher core densities, the flattening and shoulder vanishes, and the SOL density profiles become more monotonically decaying across the SOL. At the same time, the E_r magnitudes (bottom panel of Fig. 5) also decrease for higher densities, while keeping roughly the same profile shape. Here, E_r is defined as perpendicular to the LCFS, such that the expected flows are predominantly poloidal, agreeing with Fig. 3b). The E_r profiles are averaged across the poloidal extent of the probe head and the standard deviation of the averaging process is represented as shaded error bands. The expected flow magnitudes are roughly similar to the GPI results in Fig. 4, taking $v\sim E/B$ with B=2.3T at the probe location. Assuming that the drift flows contribute to plasma transport into the TSR, the decreased drift flow velocity would be in agreement with the more monotonic density profile shape at high core densities. However, in contrast the the gradual decrease of the flow velocity for higher densities seen by GPI in Fig. 4, there appears to be a marked change around $n_{dl} \approx 6e19m^{-2}$ in the E_r values closest to the LCFS. Further, an interesting difference of the SOL density profiles is the more gradual dependence of SOL density with

line integrated density in ABES compared to MPM, which sees a sharp step-up between $n_{dl}{=}7.8e19m^{\text{-}2}$ and $n_{dl}{=}10.1e19m^{\text{-}2}$.

5. FORWARD / REVERSED FIELD COMPARISON

Drift effects are best investigated by comparing forward and reversed field experiments. Previous investigations focused for technical reasons on the "low iota" configuration [11, 14], which features a connected chain of 6 islands and particularly long connection length (due to a small pitch angle). Here, we investigate the (more relevant) "Standard" configuration, which has 5 individual islands and a slightly larger pitch angle [20].

5.5. Reciprocating probes ("upstream")

Fig. 6 presents radial profiles of T_e, n_e, E_r in the SOL measured by electric probes on the MPM for a set of comparable density scan experiments in forward reversed magnetic field direction. consistently higher electron temperature $(\Delta T_e \sim 10 - 20 eV)$ is observed in forward field direction. These T_e profiles do not show the hollowness of previous investigations [5, 6, 22] as the previous experiments were performed at slightly higher iota (both from the vacuum magnetic "standard configuration" and via intrinsic toroidal plasma current). In the experiments in Fig. 6, the 5/5 island chain sits radially further outside due to the slightly smaller iota, and is thus more intersected by the divertor, including the island Opoint [22, 31]. It is further interesting to note that T_e does not vary significantly with plasma density across the measurement range.

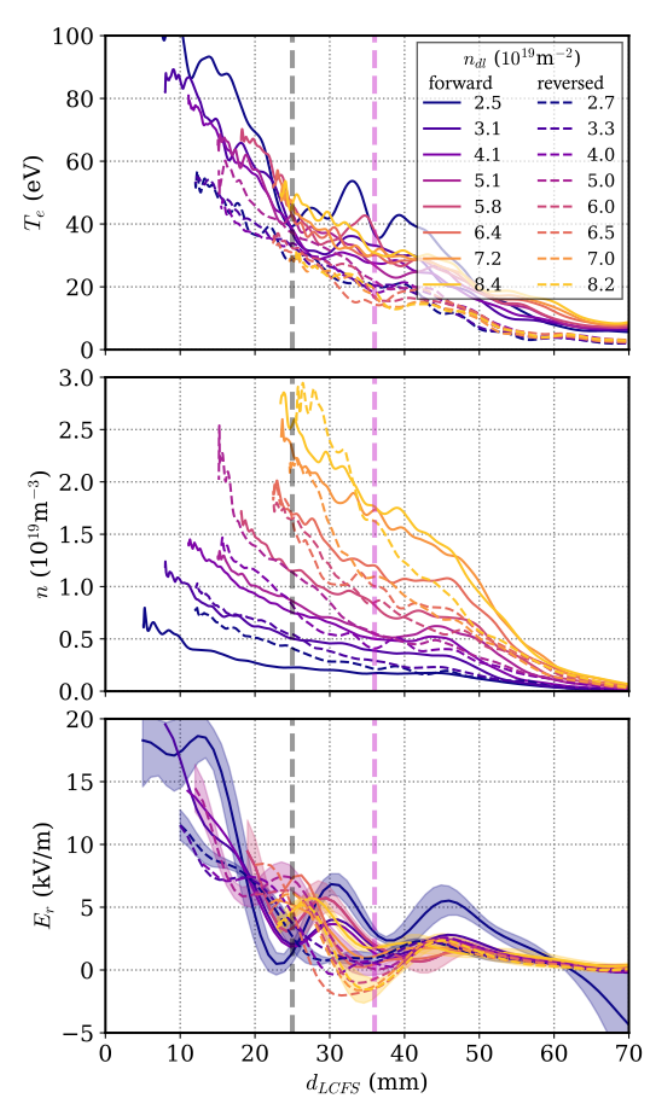


FIG 6 Radial profiles of T_e , n_e , E_r in the SOL measured by electric probes on the MPM for a comparable set of experiments in forward (solid) and reversed (dashed) field direction in the magnetic standard configuration. The gray dashed line indicates the island center; the pink dashed line the TSR boundary. Error bands of E_r are shown only for a few data sets for visual clarity.

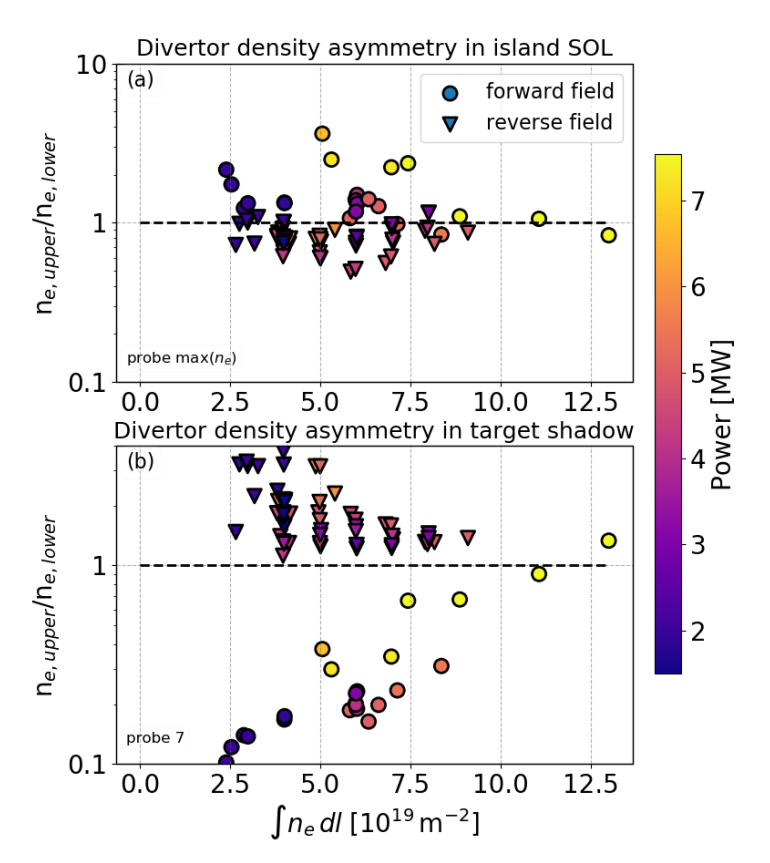


FIG 7 Ratio of electron density in the upper vs. lower divertor for Langmuir probes close to the strike line (a), and in the target shadow region (b). The vertical axis is plotted logarithmically such that asymmetries with the same magnitude but opposite direction have the same distance from the black dashed line.

The SOL densities show, similar to Fig 5, a clear correlation with the line integrated plasma density. Comparing forward and reversed field experiments, rather monotonically decaying density profiles are observed in reversed field, while the forward field profiles exhibit (similar to Fig. 5) a density shoulder outside the TSR boundary. Particularly at low line integrated densities, density profile across the island are shallow. In a quantitative comparison, at low core densities, higher SOL densities are observed in reversed field, while at high core densities higher SOL densities are found in forward field, particularly around the TSR boundary. Higher densities in the TSR in forward field are qualitatively consistent with the drift flow picture - the generally positive electric fields in forward field (see bottom panel in Fig. 6) result in upwards ExB drift at the MPM position, i.e. towards the TSR, see Fig. 2 and Fig. 3c). The dashed arrow in Fig. 3c) showing a hypothetical drift transport along flux surfaces into the TSR cannot be confirmed or denied with the current set of W7-X diagnostics.

The E_r profiles in reversed field are more difficult to interpret – while positive E_r

results in downwards flow, i.e. away from the TSR, there is a consistent region of negative E_r (and thus upwards flow) between O point and TSR boundary at high plasma densities in the reversed field case.

Considering other transport mechanism beyond the poloidal drift flows, the much steeper density profiles at high line integrated densities in Fig. 5 and Fig. 6 are expected to result in increased turbulent transport in the radial direction (and thus also into the TSR) due to higher density gradients [13]. At increasingly higher densities, the role of radial turbulent transport would increase, while the drift flow transport decreases

5.6. Divertor probes ("downstream")

The divertor probe results from the same experiments as in Fig. 6 are presented in Fig. 7, where the ratio between electron density in the upper vs lower divertor is plotted against plasma density for the strike line region in Fig. 7a) and a probe in the TSR in Fig. 7b). For the strike line region in Fig. 7a), the maximum density in each strike line region has been selected as the strike line location slightly differs between upper and lower divertor, presumably already a drift flow effect. Higher SOL densities are found in the upper divertor for line-integrated densities up to $n_{dl} \sim 7.5 \times 19 \, \text{m}^{-2}$, which is consistent with the ExB drift picture in this configuration, as the radial electric field causes a drift flow from the TSR towards the strike line. In reversed field, vice versa, higher SOL density is found at the lower divertor. The TSR probes in Fig. 7b), show a similar but quantitatively much stronger effect, again in agreement with the expectations from the simple drift picture. In forward field, drifts point into the TSR at the lower divertor and out of the TSR in the upper divertor, respectively. A clear TSR density imbalance that flips with field direction is seen in the probe data. The TSR data shows a clear decrease of the up-down asymmetry for higher plasma densities, potentially indicating the reduced impact of drift flow transport. For the strike line data in Fig. 7a), only the forward case shows a weak decrease of the asymmetry for higher densities.

5. SUMMARY

Poloidal drift flows with velocities of several km/s are ubiquitously observed in the W7-X island divertor SOL using gas puff imaging and reciprocating probes. In a simplified picture, the expected plasma convection by drifts agrees with experimentally observed features of SOL and divertor density profiles that are not expected by current models. In particular, the experimentally indicated drift transport into (away from) the TSR would be expected to cause significant density increase (decrease) in the TSR for upper (lower) divertors in forward field direction. Such up-down asymmetries are observed particularly clearly in the TSR. Drift flow velocities decrease for higher plasma densities. Accordingly, the SOL density profiles transition towards a monotonically decaying shape at high densities, and the divertor up-down asymmetries decrease. These observations emphasize the relevance of drift flows for understanding and modeling transport processes in the W7-X island divertor. Modeling tools for future stellarator reactors need to include drift physics in order to correctly predict divertor operation scenarios.

ACKNOWLEDGEMENTS

This work has been carried out within the framework of the EUROfusion Consortium, funded by the European Union via the Euratom Research and Training Programme (Grant Agreement No. 101052200—EUROfusion). Views and opinions expressed are however those of the author(s) only and do not necessarily reflect those of the European Union or the European Commission. Neither the European Union nor the European Commission can be held responsible for them.

REFERENCES

- [1] KÖNIG et al., "The divertor program in stellarators", PPCF 44 2365 (2002)
- [2] FENG et al., "Physics of island divertors as highlighted by the example of W7-AS", Nucl. Fusion 46 807 (2006)
- [3] PEDERSEN et al., "Experimental confirmation of efficient island divertor operation[...]", Nucl. Fusion 62 042022 (2022)
- [4] GAO et al., "Understanding baffle overloads observed in high-mirror configuration in W7-X", NF 60 096012 (2020)
- [5] BARBUI et al., "Measurement of plasma parameters in the divertor island [...]", Nucl. Fusion 60 106014 (2020)
- [6] KILLER et al., "Effect of toroidal plasma currents on the W7-X SOL", PPCF 62 125014 (2019)
- [7] KRÄMER-FLECKEN et al., "Investigation of turbulence rotation and radial electric [...]", PPCF 61 054003 (2019)
- [8] KILLER et al., "Characterization of the W7-X SOL using reciprocating probes, Nucl. Fusion 59 086013 (2019)
- [9] BALLINGER et al., "Gas puff imaging of filament dynamics in the SOL of W7-X" APS DPP conference (2023)
- [10] PERSEO et al., "Direct measurements of counter-streaming flows", Nucl. Fusion 59 124003 (2019)
- [11] KRIETE et al., "Effects of drifts on scrape-off layer transport in W7-X", Nucl. Fusion 63 026022 (2023)
- [12] KHARWANDIKAR "Power Exhaust Investigations in the W7-X Island Divertor", PhD Thesis, paper in prep. (2025)
- [13] PERSEO et al., "Increased power operation with water-cooled divertors at W7-X" IAEA TM Divertor (2025)
- [14] HAMMOND et al., "Drift effects on W7-X divertor heat and particle fluxes", PPCF 61 125001 (2019)
- [15] FENG et al., "First attempt to quantify W7-X island divertor plasma [...]", NF 61 106018 (2021)
- [16] BOLD et al., "Parametrisation of target heat flux distribution and study of transport [...]", Nucl. Fusion 62 106011 (2022)
- [17] BOLD et al., "Impact of spatially varying transport coefficients in EMC3-EIRENE [...]", Nucl. Fusion 64 126055 (2024)
- [18] EFFENBERG et al, "Numerical investigation of plasma edge transport and limiter heat fluxes [...]", NF 57 036021 (2017)
- [19] FENG et al., "Understanding detachment of the W7-X island divertor", Nucl. Fusion 61 086012 (2021)
- [20] WINTERS et al., "First experimental confirmation of island SOL geometry effects [...]", Nucl. Fusion 64 126047 (2024)
- [21] FENG et al., "Comparison between stellarator and tokamak divertor transport", PPCF 53 024009 (2011)
- [22] FLOM et al., "Observation of a drift-driven local transport regime in [...]", https://arxiv.org/abs/2312.01240 (2023)
- [23] KILLER et al., "Electric fields and stationary drift flows in the island divertor SOL of W7-X", NF 65 056026 (2025)
- [24] ZHANG et al., "Multi-X-point radiation and its dynamics in up/down asymmetry [...]", Nucl. Fusion 65 096032 (2025)
- [25] KILLER et al., "Turbulent transport in the scrape-off layer of Wendelstein 7-X", Nucl. Fusion 61 096038 (2021)
- [26] BAEK et al., "Gas puff imaging of plasma turbulence in the magnetic island scrape-off layer", NME 43 101937 (2025)
- [27] CSILLAG et al., "Statistical analysis of plasma filaments in the island divertor of W7-X", NF 64 016017 (2024)
- [28] TERRY et al., "First Realization of a gas puff imaging system on the Wendelstein 7-X stellarator", RSI 95 093517 (2024)
- [29] KILLER et al., "Reciprocating probe measurements in the test divertor[...]", Journal of Instrumentation 17 P03018 (2022)
- [30] CIPCIAR et al., "Fast ion temperature measurements using ball-pen probe in the W7-X SOL", submitted to PPCF (2025)
- [31] GAO et al., "Effects of toroidal plasma current on divertor power depositions on W7-X", NF 59 106015 (2019)
- [32] VECSEI et al., "Swift evaluation of electron density profiles obtained by the alkali beam [...]", RSI 92 113501 (2021)